Peridynamic Simulation of Fracture in Polycrystalline Graphene

Xuefeng Liu [1], Xiaoqiao He [2, 3], Erkan Oterkus [4], Peng Yu [1,*], Chun Lu [1,*]

[1] Department of Mechanics and Aerospace Engineering, Southern University of Science and Technology, Shenzhen, China

[2] Center for Advanced Structural Materials, City University of Hong Kong Shenzhen Research Institute, Shenzhen, China

[3] Department of Architecture and Civil Engineering, City University of Hong Kong, Hong Kong, China

[4] Peridynamics Research Centre, Department of Naval Architecture, Ocean and Marine Engineering, University of Strathclyde, Glasgow, United Kingdom

Abstract

Defect free graphene is believed to be the strongest material. However, the effective strength of engineering used large-area graphene in which defects are inevitable is actually determined by the fracture toughness, rather than the intrinsic strength that governs the breakage of atomic bonds in perfect graphene. Due to the limitations of commonly adopted experiments, conventional continuum mechanics based methods and fully atomistic simulations, fracture of polycrystalline graphene under uniaxial tensile load is explored by performing peridynamic (PD) simulations in this paper. The fracture strength, the fracture strain and the fracture toughness of polycrystalline graphene, as well as the grain size effect and the temperature effect on such quantities, are studied in this work. The results show that the fracture strength of polycrystalline graphene and the grain size follows an inverse pseudo Hall-Petch relation. The fracture strain and the fracture toughness of polycrystalline graphene decrease with a decrease in the grain size. Increasing temperature can also weaken the fracture properties of graphene. The results can provide guidelines for the applications of polycrystalline graphene in nano devices. This study also expands the application of peridynamics and presents a new way to study the fracture of graphene.

Keywords

Peridynamics; Fracture; Graphene

1. Introduction

As an excellent material, graphene has gained increasing attention from all over the

* Corresponding authors. yup6@sustech.edu.cn (Peng Yu), luc@sustech.edu.cn (Chun Lu)

This is a peer-reviewed, accepted author manuscript of the following article: Liu, X., He, X., Oterkus, E., Yu, P., & Lu, C. (Accepted/In press). Peridynamic simulation of fracture in polycrystalline graphene. Journal of Peridynamics and Nonlocal Modeling.

world. Due to its prominent mechanical, electrical and thermal properties, graphene has been applied in various areas, such as nano-devices, nano-composites, etc. Good mechanical properties of graphene are the foundation to guarantee the performance of graphene-based systems. For perfect graphene, its extremely high intrinsic strength and Young's modulus, e.g. 130.0 GPa and 1.0 TPa, respectively [1], mainly benefit from the strong atomic bonds. Now, large-area graphene can be synthesized for its practical applications, but defects are inevitable in the chemical-vapor-deposition (CVD)-synthesized graphene. Thus, the effective strength of large-area graphene is determined by the fracture toughness rather than the intrinsic strength [2].

Experimental testing and theoretical modeling are useful ways to investigate the mechanical properties (e.g. fracture) of graphene. By combining experiments and molecular dynamics (MD) simulation, Zhang et al. [2] quantified the fracture toughness of graphene as the critical stress intensity factor of $4.0 \pm 0.6\ \mathrm{MPa}\sqrt{\mathrm{m}}$ and the equivalent critical strain energy release rate of $15.9\ \mathrm{J/m^2}$. However, theoretical modeling is preferred in most studies due to the high cost of experiments and the difficulties in experimental operations.

Although classical continuum mechanics (CCM) based methods are effective and efficient to predict many mechanical behaviors (e.g. vibration and stress wave propagation, etc.) of graphene under the continuum hypothesis, they cannot directly be employed to solve discontinuity related problems (e.g. crack growth) for the reason that the spatial derivatives in CCM theory can lose its meaning at discontinuities. For discontinuity related problems such as crack propagation in graphene, MD simulation methods are mostly used for the discrete atomistic systems [2-8]. However, fully atomistic simulations (e.g. MD simulation) are prohibitively expensive to study the large-deformation and failure mechanisms at mesoscale [9]. Therefore, another method is necessary to overcome such issues.

Peridynamics, a new continuum-based theory proposed by Silling [10], can directly be used for discontinuity related problems (e.g. crack growth) ranging from macro to micro even nano scales [11]. Ren et al. [12] also developed a dual-horizon peridynamics formulation to overcome the 'ghost force' issue in the use of the original single-horizon peridynamics and applied the dual-horizon peridynamic model to the fracture of elastic solid under shear deformation [13]. Besides, inspired by the peridynamic differential operator, Ren et al. [14] proposed a nonlocal operator method for solving partial differential equations and successfully applied the model to electromagnetic waveguide problem [15]. Recently, many studies [16-23] have shown that peridynamics can be another new way to study fracture of graphene. Martowicz et al. [22] found that peridynamics can recover the physical nature of atom-scale

reactions in graphene via analyzing the wave dispersion. Based on peridynamics, Diyaroglu et al. [19] modeled the wrinkling of graphene, Madenci and Dorduncu [18] predicted the thermal expansion coefficient of graphene, and Oterkus et al. [21] investigated the fracture properties of graphene and observed the crack branching behavior in the simulation. Liu et al. [20] developed a nonlinear ordinary state-based PD coarse-grain model under isotropic assumption and captured the crack branching behavior in zigzag graphene. Considering the chiral effect on the fracture of graphene, Liu et al. [17] also developed another model by combining bond-based peridynamics and coarse-grain technique and observed the dependence of crack initiation on the chirality of graphene.

In above investigations, coarse-grained peridynamics model has been effectively adopted to investigate the fracture of large-size graphene with high efficiency. However, only crack propagation in single crystalline graphene is covered in these studies. Generally, grain boundaries are unavoidable in the CVD-synthesized graphene, and thus graphene exists in polycrystalline forms. Based on this point, a further attempt is made and fracture of polycrystalline graphene is studied via coarse-grained PD simulation in this work. In the next section, methodology employed in this study is described. Then, via coarse-grained PD simulations, fracture of pre-cracked polycrystalline graphene under uniaxial stretching and the effect of different factors (e.g. the grain size and temperature) on the fracture are presented and discussed. Finally, some concluding remarks obtained from this study are drawn.

2. Methodology

Each polycrystalline graphene sample used for the fracture investigation is considered as homogeneous and discretized as square-distributed material points. Several seeds are randomly scattered in each sample and each seed represents one grain in the sample. According to the distances between the material points and the randomly scattered seeds, polycrystalline graphene containing several grains can be obtained. For example, if the material points are closer to one seed than to other seeds in the sample, the material points then belong to the grain represented by the seed. Random chiral angles are defined for the grains in each sample. A schematic of polycrystalline graphene is shown in Fig. 1.

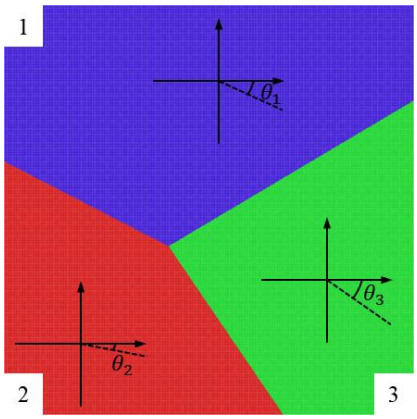

Fig. 1 A schematic to show the polycrystalline graphene sample containing 3 grains. In the sample, 1, 2, 3 and θ_1, θ_2, θ_3 stand for the grain number and the corresponding chiral angle of each grain, respectively.

The deformation of the system can be obtained via the governing equation of the material point which is written as

$$\rho_k \ddot{\mathbf{u}}_k = \int_{H_k} \boldsymbol{f}\, dV + \mathbf{b}_k \tag{1}$$

where ρ_k is the density, $\ddot{\mathbf{u}}_k$ is the acceleration vector, H_k is the corresponding horizon, $\mathbf{b}_k$ is the body force density vector, and dV is the volume of the material point, as shown in Fig. 2. $\boldsymbol{f}$ is the PD force density vector and is defined as

$$\boldsymbol{f} = \mu f_{\vec{\boldsymbol{n}}} \frac{\mathbf{y}_j - \mathbf{y}_k}{|\mathbf{y}_j - \mathbf{y}_k|} \tag{2}$$

in which $\mathbf{y}_j$ and $\mathbf{y}_k$ are the position vectors of two material points j and k after deformation, respectively, $f_{\vec{\boldsymbol{n}}}$ is the PD force density function, μ is a history-dependent scalar and is written as

$$\mu = \begin{cases} 1 & s < s_0 \\ 0 & s \geq s_0 \end{cases} \tag{3}$$

s is the stretch of the PD bond and is expressed as

$$s = \frac{|\mathbf{y}_j - \mathbf{y}_k| - |\mathbf{x}_j - \mathbf{x}_k|}{|\mathbf{x}_j - \mathbf{x}_k|} \tag{4}$$

where $\mathbf{x}_j$ and $\mathbf{x}_k$ are the position vectors of two material points j and k before deformation, respectively. When the bond stretch, s, is larger than the critical value, s_0, μ renders the PD force density to be zero, which means that the corresponding PD bond breaks and damage occurs in the PD material body.

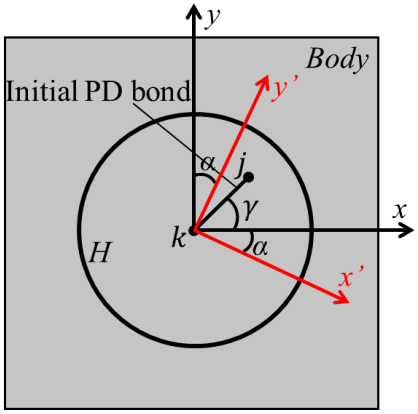

Fig. 2 Schematic of the PD material body of graphene in which the central material point *k* interacts with its neighboring material points (e.g. *j*) in the horizon *H*. The *xy* coordinate system is a global system. The *x'y'* coordinate system is a local one and can change with the chiral angle, α. *x'* and *y'* are along the zigzag and armchair edges in graphene, respectively. γ is the orientation angle of the initial PD bond *kj* relative to the global coordinate system.

A chirality-dependent PD model which was developed by Liu et al. [17] on the basis of the original bond-based PD theory is employed to describe the interaction between material points in graphene. In the model, the nonlinear and anisotropic mechanical property of single crystalline graphene is considered and the PD force density function between two material points is expressed as

$$f_{\vec{n}} = (c_2 \cos(6\beta) + c_1)s^2 + c_0 s \tag{5}$$

in which $\vec{n}$ represents the orientation of the initial PD bond relative to the local coordinate system and is denoted by the orientation angle β ($\beta = \alpha + \gamma$), as shown in Fig. 2. c_0, c_1 and c_2 are the PD parameters which are determined by the stress equivalence principle in the work by Liu et al. [17]. The critical bond stretch, s_0, is expressed as [17]

$$s_0 = s_2 \cos(6\beta) + s_1 \tag{6}$$

in which

$$s_1 = \frac{sc_z + sc_a}{2} \quad \text{and} \quad s_2 = \frac{sc_z - sc_a}{2} \tag{7}$$

where sc_z and sc_a are the critical stretches of PD bonds along the zigzag and armchair edges, respectively.

In the PD simulation of fracture of polycrystalline graphene in this study, the chirality-dependent PD model can only be used to describe the interaction between material points in each single grain. The interaction between material points in two different grains in polycrystalline graphene and the critical stretches of the corresponding PD bonds need to be considered additionally. Generally, the

expressions of the PD bond force density and the critical PD bond stretch for the PD bond crossing the grain boundary are defined as $f^i = w_A f_A + w_B f_B$ and $s_0^i = w_A s_0^A + w_B s_0^B$, respectively. In the expressions, w_A and w_B are weighted parameters which should be between 0 and 1, f_A and f_B represent the PD force densities in grains A and B, and s_0^A and s_0^B are the critical PD bond stretches in grains A and B. Different combinations of the weighted parameters can be selected to study their effect on the fracture and there should be only one correct combination for one certain case. In this work, the weighted parameters are chosen as 0.5. i.e.

$$f^i = {(f_A + f_B)}/{2} \tag{8}$$

$$s_0^i = {(s_0^A + s_0^B)}/{2} \tag{9}$$

In the simulations, the sizes of the polycrystalline graphene samples are ($W \times H$) 300 nm × 300 nm and a pre-crack with a size of ($w \times h$) 2 nm × 70 nm is positioned at the center of each sample. The grid spacing of square-distributed material points in the sample is 0.6 nm. The horizon size is chosen as 1.8 nm which is usually 3 times of the grid spacing [24]. According to Liu et al. [17], the PD parameters, i.e. c_0, c_1 and c_2 in Eq. (5) and the critical stretches, i.e. sc_z and sc_a in Eq. (7) are chosen as

$$c_0 = \frac{7.4\times10^{12}}{\pi h\delta^3},\ c_1 = -\frac{19.5\times10^{12}}{\pi h\delta^3},\ c_2 = \frac{19.2\times10^{12}}{\pi h\delta^3},\quad sc_z = 0.13 \text{ and } sc_a = 0.1. \tag{10}$$

The velocity-Verlet numerical scheme [25] is adopted with a timestep of 5 fs in the simulation. The volume-based correction method [26] is employed to minimize the surface effect in the PD simulation. It should be noted that the chirality-dependent PD model has been validated via simulation of the fracture of single crystalline graphene with different chiralities [17]. Simulations in this work are performed through running FORTRAN code in serial mode. The results such as the crack propagation forms in polycrystalline graphene are visualized by using the software OVITO [27].

3. Results and discussion

Mechanical properties and fracture characteristics of polycrystalline graphene under uniaxial load are presented and analyzed in this section. The graphene is uniaxially stretched by moving the left and right boundaries with velocities of -3 m/s and 3 m/s, respectively, and the corresponding loading rate is 2×10^7 /s. Fig. 3 presents the fracture forms and the uniaxial tensile stress-strain curves of pre-cracked polycrystalline graphene samples which contain different number of grains. Fig. 3

demonstrates that the pre-cracked graphene sample breaks in a brittle way. With each graphene sample being uniaxially stretched by moving the left and right boundaries, the uniaxial stress increases linearly with the strain. Here, the uniaxial stress and the strain are calculated as $\sigma = F/A$ and $\varepsilon = (l - l_0)/l_0$, respectively, where F is the force on the boundary, A is the cross sectional area, l is the current length, and l_0 is the initial length. When the strain reaches a critical value, the uniaxial stress reaches the maximum at the same time. After that, the graphene sample breaks into two halves in a brittle way, which is consistent with the experimental observation by Zhang et al. [2]. Besides, the maximum fracture stress (about 11.0 GPa) is substantially lower than the intrinsic strength (about 130.0 GPa) of graphene. Therefore, the results verify the fact that the strength of defective graphene is not determined by the intrinsic strength which governs the breakage of atomic bonds in perfect graphene.

Sample no.	Initial pre-cracked structure	Cracked structure	Stress-strain curve
1	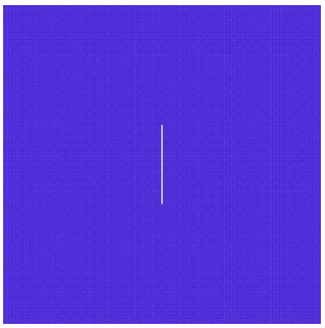	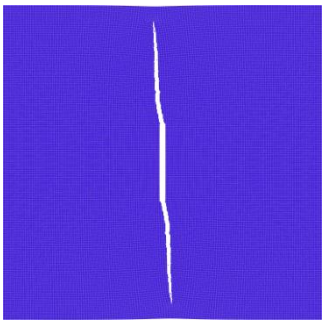	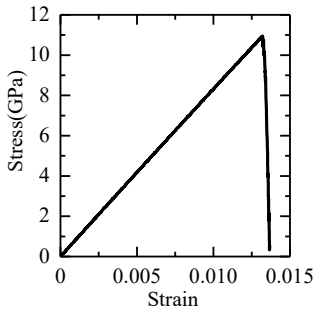
2	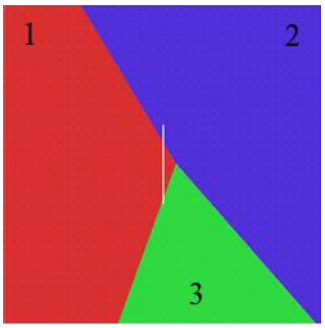	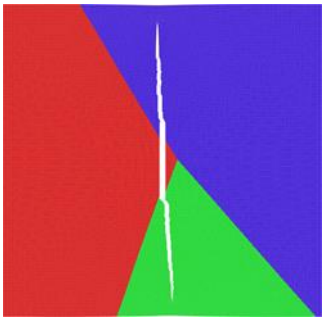	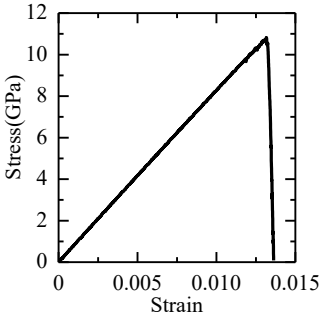
3	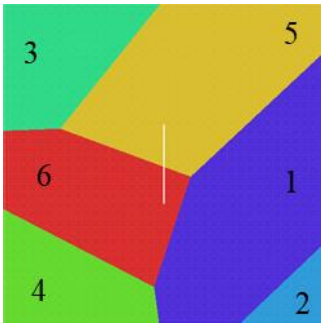	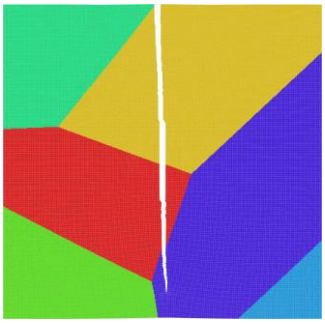	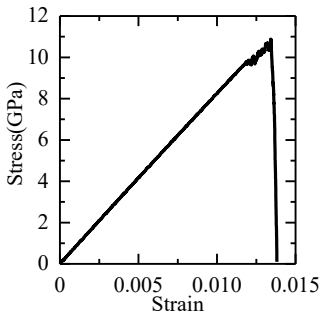

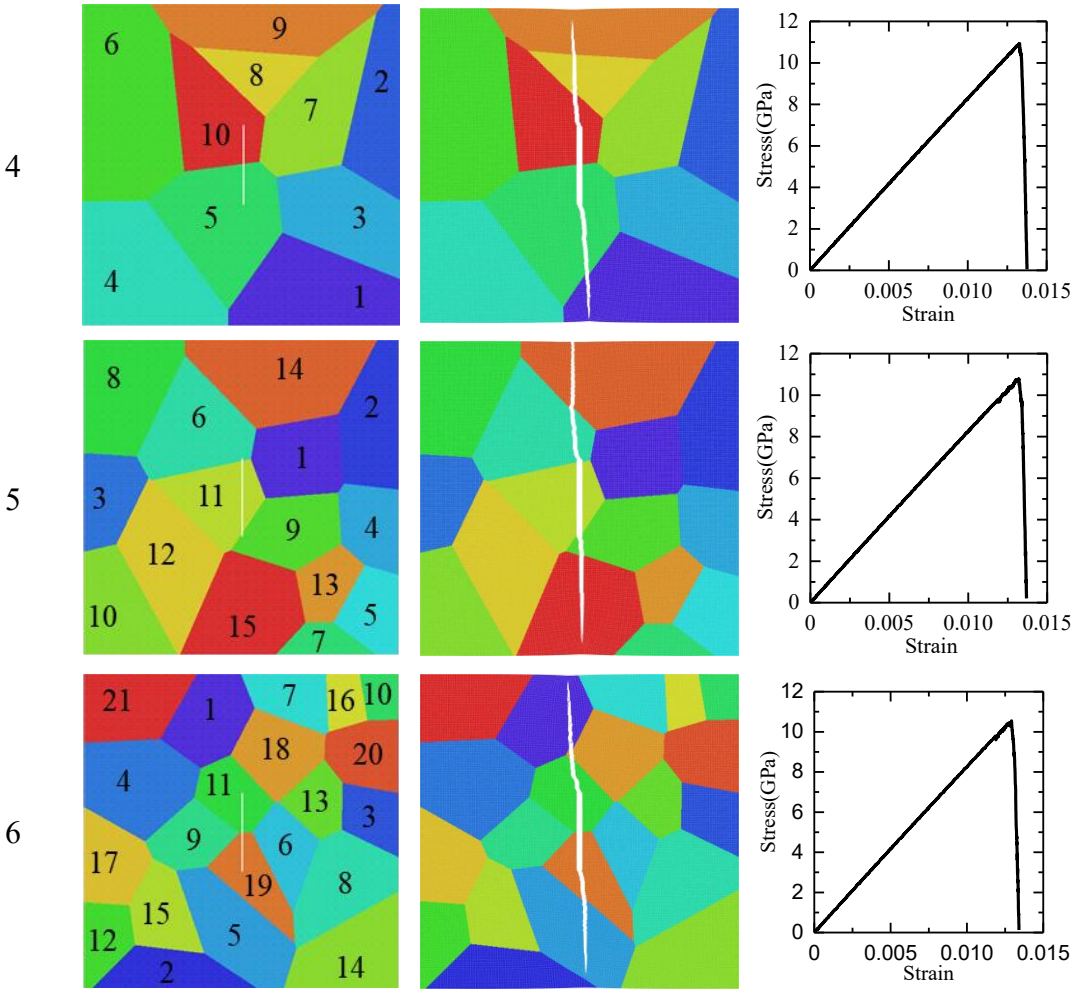

Fig. 3 Crack propagation in polycrystalline graphene with different number of grains and the corresponding stress-strain relations under uniaxial tension. The numbers in the insets represent the grain number in the corresponding polycrystalline graphene sample.

Although the global crack propagation path in graphene is perpendicular to the uniaxial stretching direction, the pre-crack initiation direction is significantly dependent on the chiral angle of the grain where the initial pre-crack tip is located, as shown in Fig. 3. This can be explained by the critical strain energy release rate for the armchair and zigzag edges in graphene, respectively. Zhang et al. [2] reported that the critical strain energy release rate is the lowest of 11.8 $\mathrm{J/m^2}$ for the zigzag edge and the highest of 12.5 $\mathrm{J/m^2}$ for the armchair edge, which means that the crack prefers to propagate along the zigzag edge. As shown in Fig. 4, the chiral angle is θ (the angle between the zigzag edge-1 and the horizontal axis) and the chiral structure in graphene shows a period of 60º. In the uniaxial stretching process, the local tensile stress (around the pre-crack tip and perpendicular to the zigzag edge) on the zigzag edge-2 is certainly larger than the one on the zigzag edge-1. Thus, the crack can

propagate more easily along the zigzag edge-2 and the angle between the crack propagation direction and the vertical axis is $30^{o}-\theta$. Therefore, it can be seen in Fig. 3 that the pre-crack initiates centro-symmetrically from the upper and lower crack tips in the single crystalline graphene (sample 1) with chiral angle of 6.8º (See Table A1 in appendix A) and the angle between the crack initiation direction and the vertical axis is about 23º. In the polycrystalline graphene samples, Fig. 4 shows that the chiral angles of the two grains where the upper and lower crack tips of the pre-crack are located are different, and this can result in different crack initiation directions. Besides, the crack propagation can also be affected due to large differences between the chiral angles of the grains in the polycrystalline graphene samples. Especially, the crack path is changed in sample 5 in Fig. 3 when the crack propagates across the grain boundary between grain 6 and grain 14. In sample 3 in Fig. 3, the chiral angle of grain 5 is larger than the one of grain 1. Correspondingly, Fig. 4 demonstrates that the crack can propagate more easily in grain 5 (e.g. the crack propagates to the upper edge faster than to the lower edge in sample 3). The large differences between the chiral angles of the grains in the polycrystalline graphene sample can also induce obvious stress oscillations before fracture occurs (e.g. the stress oscillates before it reaches the fracture stress in the stress-strain relationship of sample 3 in Fig.3). It can be understood here that the crack propagates locally depending on the chiral structure (i.e. the chiral angle of graphene) and globally depending on the uniaxial stretching direction. Therefore, the crack propagation pattern in graphene should be the consequence of the competition between the local and global level fractures, as reported by Liu et al. [3]. In addition, inter-granular fracture in polycrystalline graphene is significantly dependent on the determination of the weighted parameters in the PD model for the grain boundary. With the current PD model, the crack propagation along the interface between two grains is too short to be obviously observed from the simulation results in this work. To date, few studies can present a way to determine the weighted parameters exactly. How to obtain accurate weighted parameters is under exploration at present, which can be a further extension of the current work in the future.

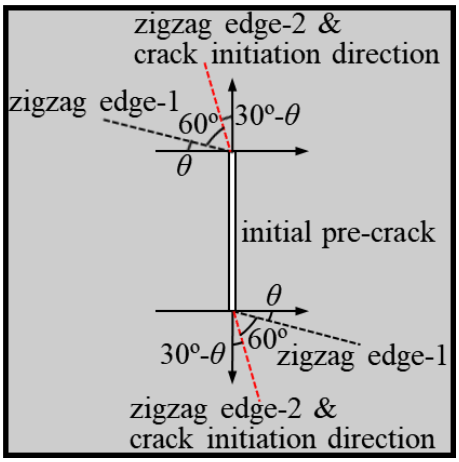

Fig. 4 Schematic to show the direction of crack initiation from the crack tip of the initial pre-crack.

The following part presents the effect of the grain size in the polycrystalline graphene sample on the mechanical properties, such as the Young's modulus in Fig. 5, and the fracture strength and the fracture strain in Fig. 6. It should be noted that the grain size is defined as $d = \sqrt{A/N}$ by assuming a square geometry for an equivalent grain in a polycrystalline graphene [7]. In the expression, A is the area of the polycrystalline graphene sample and equal to the product of its width (W) and height (H) and N is the number of grains in the polycrystalline graphene. Different grain sizes are considered by changing the number of grains in the sample of fixed size in this work. This is different from the way used by Mortazavi et al. [28] that the number of grains is fixed while the global size of the sample is changed. In the figures, each point is obtained by taking the average of five values which are collected from five independent simulations to reduce the effect of randomness.

In Fig. 5, the Young's modulus is obtained by calculating the slope of the initial linear part of the stress-strain curve (the corresponding strain is in the range of 0~0.01%). For the graphene with (or without) initial pre-crack, the Young's modulus of the single crystalline graphene is the largest. The Young's modulus slightly decreases with a decrease in the grain size. The Young's modulus of graphene without the initial pre-crack is about 0.99 TPa which matches well with the measured value (about 1.0 TPa) in the experiment by Lee et al. [1]. Compared with the grain size effect, the Young's modulus of graphene can be affected more by the initial pre-crack. The effective Young's modulus of graphene with the initial pre-crack is about 0.964 TPa.

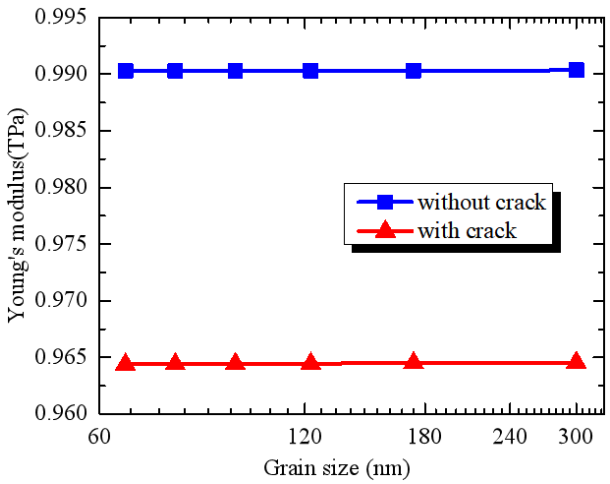

Fig. 5 The grain size effect on theYoung's modulus of polycrystalline graphene.

In Fig. 6a, the fracture strength of graphene decreases with a decrease in the grain size, which presents a similar inverse pseudo Hall-Petch relation to the one reported by Sha et al. [6]. Such relation can be explained by the weakest-link model [6] which shows that the fracture strength of a brittle material and the number of weak links in the material follows a power-law relation and the fracture strength decreases with an increase in the number of weak links. Here, the grain boundaries and the junctions formed by the grain boundaries in graphene increase with the number of grains. Thus, the weak links in graphene increase, which can lead to the reduction of fracture strength of graphene. Besides, it can be observed from Fig. 6a that the fracture strength of graphene shows very small change when the grain size is less than a certain value (e.g. 95 nm). The fracture strain of graphene and the grain size also presents a similar trend as the fracture strength *vs* the grain size does, and the fracture strain decreases with reducing the grain size, as shown in Fig. 6b. In addition, it is found that the inverse pseudo Hall-Petch relation between the fracture strength and the grain size is slightly different from the one reported by Kotakoski and Meyer [29] and Sha et al. [6]. The increasing rate of the fracture strength increases with increasing the grain size in this work but decreases in the referenced studies. Such differences may be ascribed to the range of the grain size that the grain size is larger than 65 nm in this work but smaller than 15 nm in the referenced studies.

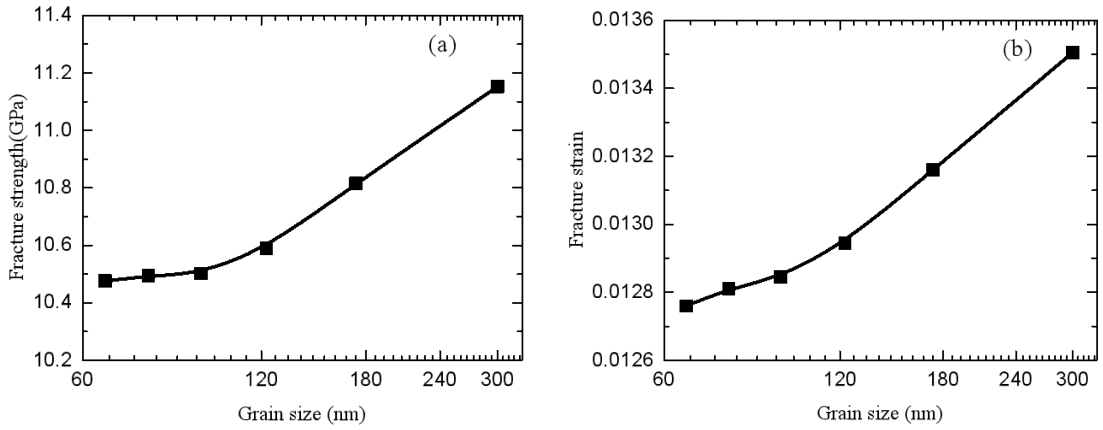

Fig. 6 Fracture strength (a) and fracture strain (b) of pre-cracked polycrystalline graphene with grains of different sizes.

In addition to the grain size effect, the fracture properties of graphene can also be affected by temperature [30]. According to the PD theory [31], the temperature effect can be considered by adding a thermal expansion coefficient related term. Thus, the PD model (i.e. eq. (5)) in this work can be rewritten as

$$f_{\vec{n}} = (c_2 \cos(6\beta) + c_1)s^2 + c_0(s + \alpha T) \tag{11}$$

where α is the thermal expansion coefficient and T is the temperature of the system. According to Moradi et al. [32], the thermal expansion coefficient of graphene is -9×10^{-6} /K when the temperature is 100 K and approaches 0 /K as the temperature increases. Besides, the thermal coefficient is 0 /K when the temperature is 0 K. Based on the PD model, dependencies of the fracture strength and the fracture strain of a pre-cracked single crystalline graphene are obtained and shown in Fig. 7. It can be seen that increasing temperature can reduce the fracture strength and the fracture strain of graphene.

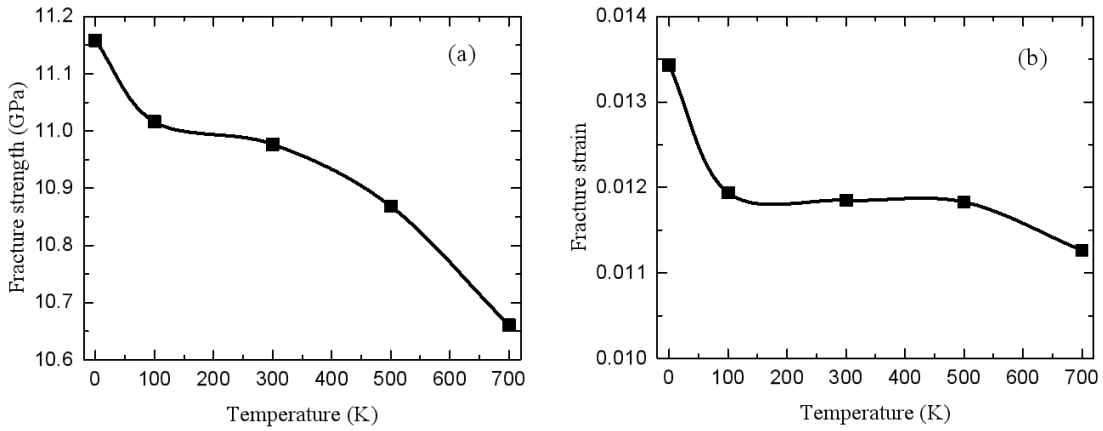

Fig. 7 Fracture strength (a) and fracture strain (b) of pre-cracked graphene at different

temperatures.

For the brittle fracture of graphene, Zhang et al. [2] verified the applicability of the classical Griffith theory of brittle fracture to graphene via combining experiment and MD simulation. For a central crack with length of $2a_0$, the critical stress, σ_c for the onset of brittle facture is a function of a_0 in the Griffith theory and the function is expressed as

$$\sigma_c = \sqrt{\frac{2\gamma E}{\pi a_0}} \tag{12}$$

where E is the Young's modulus and γ is the edge (e.g. the armchair and zigzag edges) energy of graphene. Two times of the edge energy (2γ) is equal to the critical strain energy release rate for the corresponding edge in graphene. Eq. (12) can be rewritten as $\sigma_c\sqrt{a_0} = \sqrt{2\gamma E/\pi}$, so that $\sigma_c\sqrt{a_0}$ should be a constant because the right-hand side depends on the material constants (i.e. γ and E) and the numerical constant (i.e. π). This is also consistent with the measured values in experiment [2]. Due to the brittle fracture nature of graphene, the effective strength of graphene can be indicated by the fracture toughness which is characterized by the critical stress intensity factor of fracture, $K_c = \sigma_c\sqrt{\pi a_0}$. Then, based on the length of the initial pre-crack in each graphene sample and the critical stress which can be obtained from the corresponding stress-strain relation in Fig. 3, the critical stress intensity factor of fracture of each graphene sample can be calculated.

Fig. 8 gives the relationship between the critical stress intensity factor of fracture and the grain size in the pre-cracked graphene samples. From the figure, it can be determined that the critical stress intensity factor of fracture of the pre-cracked single crystalline graphene (i.e. the number of grains equal to 1 and the grain size is 300 nm) is 3.82 $\mathrm{MPa}\sqrt{\mathrm{m}}$, which is very close to the value (about 4.0 $\mathrm{MPa}\sqrt{\mathrm{m}}$) measured in experiment [2]. Based on Eq. (12), the edge energy of graphene can be calculated as 7.4 $\mathrm{J/m^2}$, which is also close to the experimental value of 8.0 $\mathrm{J/m^2}$ (the edge energy is expressed as $\gamma = {\sigma_c}^2\pi a_0/2E = {K_c}^2/2E$ and K_c and E are selected as 3.82 $\mathrm{MPa}\sqrt{\mathrm{m}}$ and 0.99 TPa in the calculation in this work and 4.0 $\mathrm{MPa}\sqrt{\mathrm{m}}$ and 1.0 TPa in the experimental calculation, respectively). It can also be observed from the figure that the critical stress intensity factor of fracture decreases with a decrease in the grain size while it can hardly change when the grain size is less than a critical value (e.g. 95 nm). Besides, the temperature effect on the critical stress intensity factor of fracture of a pre-cracked single crystalline graphene is shown in Fig. 9 from

which it can be seen that the critical stress intensity factor can be weakened as the temperature increases.

In addition, the equi-biaxial breaking strength of pristine and polycrystalline graphene are tested as 103 GPa and 98.5 GPa, respectively, as reported by Lee et al. [33] in their experiment. Thus, it can be concluded that the fracture strength of polycrystalline graphene can slightly be reduced by the grain boundaries (about $103.0/98.5 - 1.0 = 4.6\%$). Compared with the grain boundary, the existence of the pre-crack can severely reduce the fracture strength of graphene by several folds [2]. In this study, the fracture strengths of pre-cracked single- and poly-crystalline graphene are about 11.2 GPa and 10.5 GPa, respectively. The fracture strength of the pre-cracked single-crystalline graphene is about 6.7% ($11.2/10.5 - 1.0 = 6.7\%$) higher than that of the pre-cracked polycrystalline graphene, which is consistent with the report by Lee et al. [33]. Correspondingly, the critical stress intensity factor (K_c) of the pre-cracked single-crystalline graphene is 6.7% ($3.82/3.58 - 1.0 = 6.7\%$) higher than that of the pre-cracked polycrystalline sample.

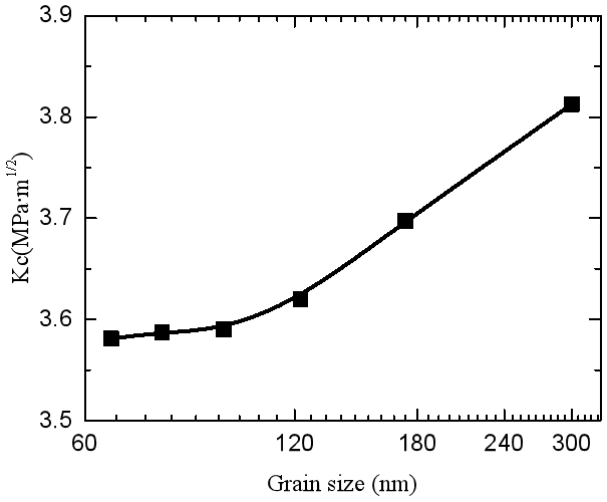

Fig. 8 Critical stress intensity factor of pre-cracked polycrystalline graphene with grains of different sizes.

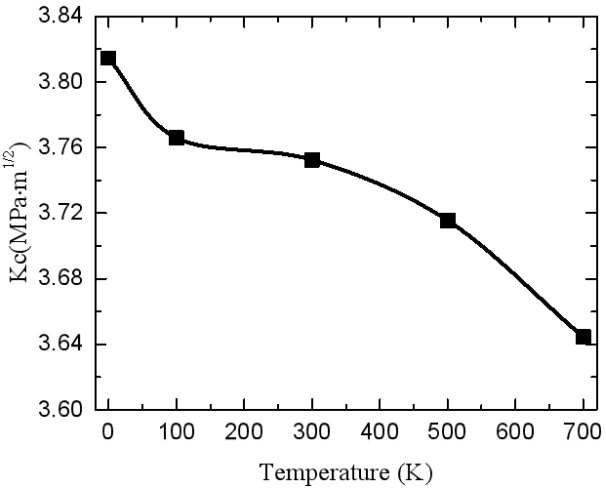

Fig. 9 Critical stress intensity factor of pre-cracked single crystalline graphene at different temperatures.

4. Conclusions

The fracture of pre-cracked polycrystalline graphene under uniaxial stretching is studied via coarse-grained PD simulation. The following several concluding remarks can be drawn from this study. The local crack propagation such as the crack initiation or the crack crossing a grain boundary depends on the chiral angle while the global crack path is perpendicular to the uniaxial stretching direction. Therefore, the fracture of graphene is the result of the local and global level fractures. The fracture strength decreases with a decrease in the grain size, which follows an inverse pseudo Hall-Petch relation and can be explained by the weakest-link model that the increasing weak links in graphene due to the increase of the number of grains can reduce the fracture strength of polycrystalline graphene. Besides, the fracture strain and the critical stress intensity factor of fracture reduce as the grain size decreases. The change of the three fracture related quantities is very limited when the grain size is less than a critical value. The three fracture related quantities can be reduced by increasing the temperature. In this study, the critical stress intensity factor of fracture and the edge energy of pre-cracked single crystalline graphene are calculated as 3.82 $\mathrm{MPa}\sqrt{\mathrm{m}}$ and 7.4 $\mathrm{J/m^2}$, respectively, which are very close to the experimental values (i.e. 4.0 $\mathrm{MPa}\sqrt{\mathrm{m}}$ and 8.0 $\mathrm{J/m^2}$). This study verifies the fact that the effective strength of defective graphene is determined by the fracture toughness rather than the intrinsic strength of perfect graphene and the obtained results are useful for the application of graphene in many nano systems. Moreover, further extensions can be made for the application of peridynamics through this work.

Acknowledgements

Dr. Xuefeng Liu is grateful for the financial support from the Basic and Applied Basic Research Foundation of Guangdong Province (Grant No. 2020A1515110296). Dr. Peng Yu is grateful for the financial support from the Shenzhen Science and Technology Innovation Commission (Grant No. JCYJ20170817110214213). Prof. Xiaoqiao He is grateful for the financial support from the Shenzhen Science and Technology Innovation Commission (Grant No. JCYJ20190808175607486). Numerical simulations in this work are supported by Center for Computational Science and Engineering at Southern University of Science and Technology.

Appendix A

The chiral angle of each grain in polycrystalline graphene samples in Fig. 3 is presented in the table below.

Table A1. The chiral angle information of each grain in polycrystalline graphene samples in Fig. 3.

Unit: degree

Grain no. \ Sample no.	1	2	3	4	5	6
1	6.8	4.1	5.4	9.0	10.6	19.0
2		15.5	6.6	4.0	18.5	25.4
3		15.4	1.1	2.1	0.4	23.2
4			2.2	17.7	19.4	0.8
5			22.9	6.4	29.8	3.2
6			24.5	10.4	13.1	17.1
7				24.0	1.3	23.0
8				3.7	12.2	19.7
9				16.5	3.5	17.9
10				9.4	4.3	8.8
11					17.6	10.6
12					19.8	14.1
13					6.7	9.1
14					0.0	29.4
15					29.0	5.5
16						12.3
17						18.6
18						14.7
19						2.7

20	29.9
21	15.8

Conflicts of interest

There is no conflict of interest in this work.

References

[1] C. Lee, X. Wei, J.W. Kysar, J. Hone, Measurement of the elastic properties and intrinsic strength of monolayer graphene, Science, 321 (2008) 385-388.

[2] P. Zhang, L. Ma, F. Fan, Z. Zeng, C. Peng, P.E. Loya, Z. Liu, Y. Gong, J. Zhang, X. Zhang, P.M. Ajayan, T. Zhu, J. Lou, Fracture toughness of graphene, Nature Communications, 5 (2014) 3782.

[3] X. Liu, Z. Bie, J. Wang, L. Sun, M. Tian, E. Oterkus, X. He, Investigation on fracture of pre-cracked single-layer graphene sheets, Computational Materials Science, 159 (2019) 365-375.

[4] M.Z. Hossain, T. Ahmed, B. Silverman, M.S. Khawaja, J. Calderon, A. Rutten, S. Tse, Anisotropic toughness and strength in graphene and its atomistic origin, Journal of the Mechanics and Physics of Solids, 110 (2018) 118-136.

[5] Z.D. Sha, Q. Wan, Q.X. Pei, S.S. Quek, Z.S. Liu, Y.W. Zhang, V.B. Shenoy, On the failure load and mechanism of polycrystalline graphene by nanoindentation, Scientific Reports, 4 (2014) 7437.

[6] Z.D. Sha, S.S. Quek, Q.X. Pei, Z.S. Liu, T.J. Wang, V.B. Shenoy, Y.W. Zhang, Inverse pseudo Hall-Petch relation in polycrystalline graphene, Scientific Reports, 4 (2014) 5991.

[7] B. Mortazavi, G. Cuniberti, Atomistic modeling of mechanical properties of polycrystalline graphene, Nanotechnology, 25 (2014) 215704.

[8] A. Cao, J. Qu, Atomistic simulation study of brittle failure in nanocrystalline graphene under uniaxial tension, Applied Physics Letters, 102 (2013).

[9] L. Ruiz, W. Xia, Z. Meng, S. Keten, A coarse-grained model for the mechanical behavior of multi-layer graphene, Carbon, 82 (2015) 103-115.

[10] S.A. Silling, Reformulation of elasticity theory for discontinuities and long-range forces, Journal of the Mechanics and Physics of Solids, 48 (2000) 175-209.

[11] A. Ahadi, S. Melin, Capturing nanoscale effects by peridynamics, Mechanics of Advanced Materials and Structures, 25 (2017) 1115-1120.

[12] H. Ren, X. Zhuang, Y. Cai, T. Rabczuk, Dual-horizon peridynamics, International Journal for Numerical Methods in Engineering, 108 (2016) 1451-1476.

[13] H. Ren, X. Zhuang, T. Rabczuk, A new peridynamic formulation with shear deformation for elastic solid, Journal of Micromechanics and Molecular Physics, 01 (2016).

[14] H. Ren, X. Zhuang, T. Rabczuk, A nonlocal operator method for solving partial differential equations, Computer Methods in Applied Mechanics and Engineering, 358 (2020).

[15] T. Rabczuk, H. Ren, X. Zhuang, A Nonlocal Operator Method for Partial Differential Equations with Application to Electromagnetic Waveguide Problem, Computers, Materials & Continua, 59 (2019) 31-55.

[16] S.A. Silling, M. Fermen-Coker, Peridynamic model for microballistic perforation of multilayer graphene, Theoretical and Applied Fracture Mechanics, 113 (2021).

[17] X. Liu, X. He, L. Sun, J. Wang, D. Yang, X. Shi, A chirality-dependent peridynamic model for the fracture analysis of graphene sheets, Mechanics of Materials, 149 (2020).

[18] E. Madenci, A. Barut, M. Dorduncu, Peridynamics for Predicting Thermal Expansion Coefficient of Graphene,

in: 2019 IEEE 69th Electronic Components and Technology Conference (ECTC), 2019, pp. 825-833.
[19] C. Diyaroglu, D. Behera, E. Madenci, Y. Kaya, G. Kedziora, D. Nepal, Peridynamic Modeling of Wrinkling in a Graphene Layer, in: AIAA Scitech 2019 Forum, 2019.
[20] X. Liu, X. He, J. Wang, L. Sun, E. Oterkus, An ordinary state-based peridynamic model for the fracture of zigzag graphene sheets, Proceedings of the Royal Society A: Mathematical, Physical and Engineering Sciences, 474 (2018) 20180019.
[21] E. Oterkus, C. Diyaroglu, N. Zhu, S. Oterkus, E. Madenci, Utilization of Peridynamic Theory for Modeling at the Nano-Scale, in: Nanopackaging: From Nanomaterials to the Atomic Scale, 2015, pp. 1-16.
[22] A. Martowicz, W.J. Staszewski, M. Ruzzene, T. Uhl, Peridynamics as an analysis tool for wave propagation in graphene nanoribbons, in: Sensors and Smart Structures Technologies for Civil, Mechanical, and Aerospace Systems 2015, 2015, pp. 94350I.
[23] X. Liu, X. He, C. Lu, E. Oterkus, Peridynamic modeling at nano-scale, in: Peridynamic Modeling, Numerical Techniques, and Applications, 2021, pp. 355-370.
[24] S.A. Silling, E. Askari, A meshfree method based on the peridynamic model of solid mechanics, Computers & Structures, 83 (2005) 1526-1535.
[25] W.C. Swope, H.C. Andersen, P.H. Berens, K.R. Wilson, A computer simulation method for the calculation of equilibrium constants for the formation of physical clusters of molecules: Application to small water clusters, The Journal of Chemical Physics, 76 (1982) 637-649.
[26] Q.V. Le, F. Bobaru, Surface corrections for peridynamic models in elasticity and fracture, Computational Mechanics, 61 (2017) 499-518.
[27] A. Stukowski, Visualization and analysis of atomistic simulation data with OVITO–the Open Visualization Tool, Modelling and Simulation in Materials Science and Engineering, 18 (2010).
[28] B. Mortazavi, M. Silani, E.V. Podryabinkin, T. Rabczuk, X. Zhuang, A.V. Shapeev, First-Principles Multiscale Modeling of Mechanical Properties in Graphene/Borophene Heterostructures Empowered by Machine-Learning Interatomic Potentials, Advanced Materials, 33 (2021) e2102807.
[29] J. Kotakoski, J.C. Meyer, Mechanical properties of polycrystalline graphene based on a realistic atomistic model, Physical Review B, 85 (2012).
[30] M.Q. Chen, S.S. Quek, Z.D. Sha, C.H. Chiu, Q.X. Pei, Y.W. Zhang, Effects of grain size, temperature and strain rate on the mechanical properties of polycrystalline graphene – A molecular dynamics study, Carbon, 85 (2015) 135-146.
[31] E. Madenci, E. Oterkus, Peridynamic Theory and Its Applications, Springer, New York, 2014.
[32] Z. Moradi, M. Vaezzadeh, M. Saeidi, Temperature-dependent thermal expansion of graphene, Physica A: Statistical Mechanics and its Applications, 512 (2018) 981-985.
[33] G.H. Lee, R.C. Cooper, S.J. An, S. Lee, A. van der Zande, N. Petrone, A.G. Hammerberg, C. Lee, B. Crawford, W. Oliver, J.W. Kysar, J. Hone, High-strength chemical-vapor-deposited graphene and grain boundaries, Science, 340 (2013) 1073-1076.